THE JOURNAL OF BIOLOGICAL CHEMISTRY VOL. 286, NO. 47, pp. 40857–40866, November 25, 2011

Involvement of ATP-sensitive Potassium (K_{ATP}) Channels in the Loss of Beta-cell Function Induced by Human Islet Amyloid Polypeptide*[S]

Received for publication, February 18, 2011, and in revised form, October 4, 2011 Published, JBC Papers in Press, October 7, 2011, DOI 10.1074/jbc.M111.232801

Maud Soty[‡§], Montse Visa[‡§], Sergi Soriano[§¶], María del Carmen Carmona[‡], Ángel Nadal[§¶], and Anna Novials[‡§1]

From the [‡]Diabetes and Obesity Laboratory, Institut d'Investigacions Biomèdiques August Pi i Sunyer (IDIBAPS), Hospital Clinic de Barcelona, 08036 Barcelona, the [¶]Instituto de Bioingeniería, Universidad Miguel Hernández, 03202 Elche, and the [§]Centro de Investigación Biomédica en Red de Diabetes y Enfermedades Metabólicas Asociadas (CIBERDEM), 08017 Barcelona, Spain

Islet amyloid polypeptide (IAPP) is a major component of amyloid deposition in pancreatic islets of patients with type 2 diabetes. It is known that IAPP can inhibit glucose-stimulated insulin secretion; however, the mechanisms of action have not yet been established. In the present work, using a rat pancreatic beta-cell line, INS1E, we have created an *in vitro* model that stably expressed human *IAPP* gene (hIAPP cells). These cells showed intracellular oligomers and a strong alteration of glucose-stimulated insulin and IAPP secretion. Taking advantage of this model, we investigated the mechanism by which IAPP altered beta-cell secretory response and contributed to the development of type 2 diabetes. We have measured the intracellular Ca^{2+} mobilization in response to different secretagogues as well as mitochondrial metabolism. The study of calcium signals in hIAPP cells demonstrated an absence of response to glucose and also to tolbutamide, indicating a defect in ATP-sensitive potassium (K_{ATP}) channels. Interestingly, hIAPP showed a greater maximal respiratory capacity than control cells. These data were confirmed by an increased mitochondrial membrane potential in hIAPP cells under glucose stimulation, leading to an elevated reactive oxygen species level as compared with control cells. We concluded that the hIAPP overexpression inhibits insulin and IAPP secretion in response to glucose affecting the activity of K_{ATP} channels and that the increased mitochondrial metabolism is a compensatory response to counteract the secretory defect of beta-cells.

Type 2 diabetes is characterized by impaired insulin secretion with a progressive decline in beta-cell mass and function (1, 2). A main characteristic of type 2 diabetes is the extracellular accumulation of amyloid fibrils in pancreatic islets (3, 4). The main component of these deposits is the islet amyloid polypeptide (IAPP).[2] Specifically, human IAPP (hIAPP) but not rodent IAPP is amyloidogenic (5). Pancreatic beta-cells co-express and co-secrete IAPP and insulin in response to several secretagogue stimuli (6–8). It is well established that IAPP is implicated in the pathogenesis of diabetes because it forms amyloid deposits leading to beta-cell death (9–12). In addition, although different studies have demonstrated that IAPP can inhibit glucose-stimulated insulin secretion (GSIS) (13–15), the mechanisms of action have not been established.

In pancreatic beta-cells, GSIS depends critically on the activity of ATP-sensitive potassium channels (K_{ATP}), which serve as a coupling factor between changes in glucose metabolism and membrane electrical activity (16, 17). These channels are hetero-octameric complexes comprising four inward-rectifier potassium ion channels (Kir6.2) and four regulatory sulfonylurea receptors (SUR1) (18). Gain-of-function mutations of Kir6.2 are associated with defective GSIS and the development of type 2 diabetes (19, 20), whereas loss of function mutations of Kir6.2 and SUR1 are the most common causes of congenital hyperinsulinism of infancy, a disease characterized by inappropriate insulin secretion and a severe hypoglycemia (21–23). In pancreatic beta-cells, K_{ATP} channel activity is modulated by the ATP/ADP ratio, which largely depends on ATP production by mitochondrial respiratory chain through oxidative phosphorylation (OXPHOS). In the presence of higher glucose metabolism, and consequently increased levels of ATP, the K_{ATP} channels close, resulting in depolarization of the plasma membrane (24). This results in the opening of the voltage-gated calcium channel (VCC) and consequently increased concentration of intracellular Ca^{2+} ($[Ca^{2+}]_i$), provoking the exocytosis of insulin vesicles.

Over the last few years, several authors have debated whether soluble IAPP oligomers or amyloid fibrils are toxic species responsible for beta-cell death as recently reviewed in Ref. 25. Recently, it has become possible to detect the toxic form of hIAPP oligomers with specific antibodies that do not cross-react with IAPP soluble monomers or amyloid fibrils (26, 27). Using this technique, Gurlo *et al.* (28) detected the presence of IAPP oligomers in insulin vesicles and mitochondrial membranes of hIAPP transgenic mice.

Recently, Zhu *et al.* (29) investigated the effects of extracellular hIAPP treatment on the activation of VCCs, as well as

* This work was supported by Fondo de Investigaciones Sanitarias (FIS) Grant PI08/0088, the Sardà Farriol Research Program, and CIBER de Diabetes y Enfermedades Metabólicas Asociadas (CIBERDEM), which is an initiative of the Instituto de Salud Carlos III (ISCIII; Ministerio de Ciencia e Innovación).

[S] The on-line version of this article (available at http://www.jbc.org) contains supplemental Figs. S1–S4.

[1] To whom correspondence should be addressed: Diabetes and Obesity Laboratory, CEK, planta 5, Calle Rosselló 149-153, 08036 Barcelona, Spain. Tel.: 34-93-2275400 (Ext. 4153); Fax: 34-93-3129403; E-mail: anovials@clinic.ub.es.

[2] The abbreviations used are: IAPP, islet amyloid polypeptide; hIAPP, human IAPP; rIAPP, rat IAPP; GSIS, glucose-stimulated insulin secretion; VCC, voltage-gated calcium channel; FCCP, carbonyl cyanide *p*-trifluoromethoxyphenylhydrazone; OXPHOS, oxidative phosphorylation; ROS, reactive oxygen species; ER, endoplasmic reticulum.

$[Ca^{2+}]_i$ and insulin secretion in rat islets. They found that VCCs were inhibited by high concentration of extracellular hIAPP, and they proposed that the reduction of GSIS in hIAPP-treated islets is the result of IAPP inhibition of VCCs (29). The mechanism was not described, but the authors suggested that it could also be involved in the activity of K_{ATP} channels.

The main objective of this work is to investigate whether hIAPP overexpression could affect beta-cell function and by which mechanisms. In the present study, we obtained a beta-cell line that stably overexpressed the human *IAPP* gene (hIAPP cells). At first, we observed that hIAPP overexpression induced the formation of intracellular oligomers and altered beta-cell function. Indeed, hIAPP cells showed a defect in insulin and IAPP secretion in response to glucose. Then, to determine by which mechanism hIAPP alters beta-cell secretory function, we studied the effects of hIAPP overexpression on $[Ca^{2+}]_i$ mobilization in response to glucose or sulfonylurea drug and mitochondrial metabolism.

EXPERIMENTAL PROCEDURES

Establishment of Stable Cell Line Overexpressing hIAPP and Cell Culture

The hIAPP and rIAPP transcripts were amplified by polymerase chain reaction (PCR), using as template the construct described previously (30) or INS1E cells, respectively. The amplified fragments were ligated into the EcoRI and EcoRV sites of pcDNA3 for the construction of pcDNA3-hIAPP and pcDNA3-rIAPP, respectively. The rat pancreatic beta-cell line INS1E was plated at a density of 1×10^6 cells per 100-mm diameter culture dish in RPMI 1640 medium containing 11.1 mM glucose and supplemented with 10% fetal bovine serum, 2 mmol/liter L-glutamine, 5 μmol/liter β-mercaptoethanol, 100 units/ml penicillin, and 100 μg/ml streptomycin at 37 °C with 5% CO_2. After 48 h, the cells were transfected with 10 μg of human *IAPP* gene plasmid DNA, rIAPP plasmid DNA, or pcDNA3 using Lipofectamine. Two days after transfection, 800 μg/ml Geneticin was added to culture medium. Two weeks later, Geneticin-resistant colonies were picked, and colonies were expanded into stable cell lines in the presence of 200 μg/ml Geneticin.

Lentiviral Production and Titration

Rat islets were infected by lentivirus construct containing hIAPP cDNA under the control of its own promotor. The hIAPP gene promotor was obtained by digestion of pGL3 plasmids constructs (31), and the cDNA was amplified by PCR using as template; the construct was as described previously (30). The pLenti-hIAPP was constructed using the pLenti6/V5 Directional TOPO® cloning kit (Invitrogen) according to the manufacturer's protocol. pLenti6/UbC/V5-GW/LacZ (pLenti-LacZ) was used as control. Then, virus constructs were co-transfected with ViraPower™ packaging plasmid mixture: pLP1, pLP2, and pLP/VSV-G (Invitrogen) into 293FT cells using Lipofectamine 2000. The viral titer was determined by transduction of mPac cells with serial dilutions of the viral supernatant and colony counting after blasticidin selection (10 μg/ml).

Islets Isolation, Culture, and Infection

Islets were obtained from Wistar rats, isolated through collagenase perfusion and Histopaque gradient (Sigma), and cultured as described previously (32). Infection was performed 24 h after isolation. Briefly, 200 islets were resuspended in 2 ml of culture medium at 5.5 mM glucose containing virus particles at a multiplicity of infection of 600 and Polybrene to a final concentration of 8 μg/ml. The next day, the culture medium was refreshed, and islets were maintained in culture during 6 days before insulin secretion studies.

Transmission Electron Microscopy

Ultrastructure Observations—Cells were fixed with 2.5% glutaraldehyde for at least 2 h at 4 °C, washed in phosphate buffer and postfixed in 1% osmium tetroxide for 1 h at 4 °C, dehydrated in a graded acetone series, and embedded in epoxy resin (Durcupan). Semithin sections were cut with a glass knife at 1–3 μm and stained with methylene blue. For electron microscopy, ultrathin sections (70–90 nm) were cut on an ultramicrotome (Reichert Ultracut E; Leica) using a diamond knife (Diatome) and collected on 200-mesh copper or gold grids. Staining was performed on drops of 1% aqueous uranyl acetate followed by Reynolds's lead citrate. Ultrastructural analyses were performed in a Jeol-1010 electron microscope at 80 kV, and images were acquired with a Gatan Bioscan 972 camera.

Immunolabeling—Ultrathin sections for single and double immunostaining were cut and picked up on 200-mesh gold grids and immunolabeled. The sections were first etched on droplets of sodium metaperiodate for 30 min (9) and washed in five changes of deionized distilled water. The sections were then incubated in Tris-buffered saline (TBS) containing 1% bovine serum albumin (BSA), 20 mM glycine, and 150 mM NaCl for 30 min to prevent nonspecific binding followed by incubation with the primary antibody anti-oligomer (Invitrogen) for 2 h at room temperature and then incubated with goat anti-rabbit (British BioCell International) gold conjugate (15 nm) diluted 1:25 for 1 h at room temperature. Control sections were treated identically except for omission of the primary antibody. Sections were counterstained for 15 min in uranyl acetate and for 5 min in lead citrate.

RNA Isolation and Real-time PCR

Total RNA was extracted using TRIZOL reagent (Invitrogen) following the manufacturer's instructions. Thereafter, cDNA was synthesized from 2 μg of total RNA using SuperScript III reverse transcriptase (Invitrogen). The genes were amplified using SYBR Green PCR core reagents (Eurogentec). Real-time PCR was carried with 50 ng of cDNA in a Light Cycler 480 II sequence detection system (Roche Applied Science) following the manufacturer's instructions. A standard curve of each primer set was generated from serial dilutions of cDNA. PCR products were verified using dissociation curve analysis after the run using SDS software (Roche Applied Science). Expression levels were normalized to TATA box-binding protein (TBP) or glyceraldehyde-3-phosphate dehydrogenase (GAPDH) mRNA and represented in arbitrary units.

Immunodetection

Cells were fixed with 10% formalin. Then, cells were permeabilized and blocked with PBS containing 0.1% BSA and 0.1% Triton X-100 and PBS with 1% BSA, respectively. After overnight incubation at 4 °C with rabbit anti-IAPP (1/100, Biochem), cells were incubated for 1 h with Cy3 donkey anti-rabbit IgG antibody (1/500; GE Healthcare; red fluorescence). Hoechst 33258 (1/5000; Sigma) was used for nuclear counterstaining. Images were captured using a fluorescence microscope (DMRB; Leica).

Insulin and IAPP Secretion

Cells or islets were preincubated in HEPES-buffered Krebs-Ringer bicarbonate medium without glucose for 2 h at 37 °C with 5% CO_2. Then, the medium was substituted by the same medium but supplemented with 2.8 or 16.7 mM glucose or 30 mM KCl at 37 °C with 5% CO_2. At the end of the experiment, the supernatant was recovered and centrifuged to avoid cell contamination to measure insulin and IAPP release, and cells or islets were extracted with acid-ethanol solution to measure insulin and IAPP content. Insulin and IAPP release and content were determined by insulin ELISA (Mercodia) and amylin ELISA (Millipore), respectively.

Apoptosis Assay

Cells were stained with annexin V-FITC and propidium iodide using an annexin V-FITC apoptosis detection kit (BD Biosciences). Samples were analyzed by FACS within 1 h on a FACSCalibur with Cell Quest software (BD Biosciences). FACS gating based on forward and side scatter of 20,000 cells was included for analysis. Annexin V-FITC- and propidium iodide-negative cells were considered as viable, annexin V-FITC-positive cells were considered as early apoptotic, and those positive for both annexin V-FITC and propidium iodide were considered as late apoptotic or dead cells.

Recording Intracellular Calcium ($[Ca^{2+}]_i$)

Before the assay, cells were placed overnight at 2.8 mM glucose. Cells were loaded with 5 μM fura 2-AM (Molecular Probes) for at least 1 h at 37 °C and 5% CO_2. Cells were placed in a chamber mounted on the microscope stage and perfused at a rate of 1.5 ml/min with a modified Ringer's solution (33) containing glucose, KCl, or tolbutamide. Calcium records were obtained by imaging intracellular calcium under an inverted epifluorescence microscope as described previously (33). Fluorescence changes were expressed as the ratio of fluorescence at 340 and 380 nm (F_{340}/F_{380}), and the increment of fluorescence ($\Delta F_{340}/F_{380}$) was obtained by subtracting the mean basal fluorescence levels in the absence of stimulus (2.8 mM glucose) from the fluorescence value during the stimulus (16.7 mM glucose, 30 mM KCl, or 100 μM tolbutamide).

Oxygen (O_2) Consumption

Before the assay, cells were placed overnight at 2.8 mM glucose. O_2 consumption measurements were performed on live cell suspension. Cells were scraped, and approximately three million cells were placed into an oxymeter chamber of an Oxygraph-2k (Oroboros Instruments) in 2 ml of RPMI medium (2.8 mM glucose) at 37 °C and stabilized for at least 10 min without drugs. At first, the O_2 consumption was evaluated by raising the glucose concentration in the chamber from 2.8 to 16.7 mM. After recording the respiration in the absence of drugs, the uncoupled respiration was determined in the presence of the ATP synthase inhibitor, oligomycin (4 μg/ml) (Sigma-Aldrich). The maximum respiration of cells induced with 0.5 μM carbonyl cyanide *p*-trifluoromethoxyphenylhydrazone (FCCP, Sigma-Aldrich) was also measured. Prior to the assay, air calibration was performed according to the manufacturer's protocol.

ATP Measurement

Before the assay, cells were placed overnight in 2.8 mM glucose. Cells were disrupted by passive lysis buffer (Promega). Following a 20-min incubation, extracts were centrifuged (10,000 $\times$ *g*, 5 min) at 4 °C. ATP was measured in duplicate using a luciferin-luciferase bioluminescent assay (Promega). Light emission was recorded for 30 s using a photon-counting luminometer (Turner BioSystems). ATP concentration was obtained by comparison with known standards (0–100 pmol) prepared in parallel with the cell extracts.

Western Blot Analysis

Cultured cells were washed twice with ice-cold PBS, scraped, and resuspended immediately in lysis buffer containing: 5 mM EDTA, 50 mM Tris-HCl, 150 mM NaCl, 1% Triton X-100, 10 mM sodium phosphate, 10 mM sodium fluorite, 10% protease inhibitor mixture (Sigma-Aldrich). Protein content in the lysate was measured using the Bio-Rad Protein Assay kits (Bio-Rad). Protein samples (30 μg) were subjected to SDS-PAGE and transferred to PVDF membranes (PerkinElmer Life Sciences). Then, the membranes were blocked with 2% nonfat dry milk, and they were incubated with anti-OXPHOS total antibody (1/500, MitoSciences) or anti-actin antibody (1/1000) before being incubated with the appropriate HRP-conjugated antibodies (GE Healthcare). Protein bands were revealed by using the ECL chemiluminescence reagents kit (Pierce).

Mitochondrial Membrane Potential ($\Delta\psi_m$) Measurement

Before the assay, cells were placed overnight in 2.8 mM glucose. $\Delta\psi_m$ was evaluated by raising the glucose concentration from 2.8 to 16.7 mM using a specific probe: rhodamine-123 (Molecular Probes). This indicator dye accumulates in mitochondria in proportion to $\Delta\psi_m$. $\Delta\psi_m$ was monitored using the same imaging system described in Ref. 33 with conventional fluorescein filters (34, 35).

Reactive Oxygen Species (ROS) Assay

Before the assay, cells were placed overnight in 2.8 mM glucose. ROS production was evaluated by raising the glucose concentration from 2.8 to 16.7 mM and using a specific probe: 5-(and-6)-chloromethyl-2′,7′-dichlorodihydrofluorescein diacetate, acetyl ester (CM-H_2DCFDA) (Molecular Probes). The fluorescence intensity is proportional to the ROS levels within the cell cytosol and was detected using a fluorometric plate reader at 480/530 nm (Infinite® 200, Tecan).

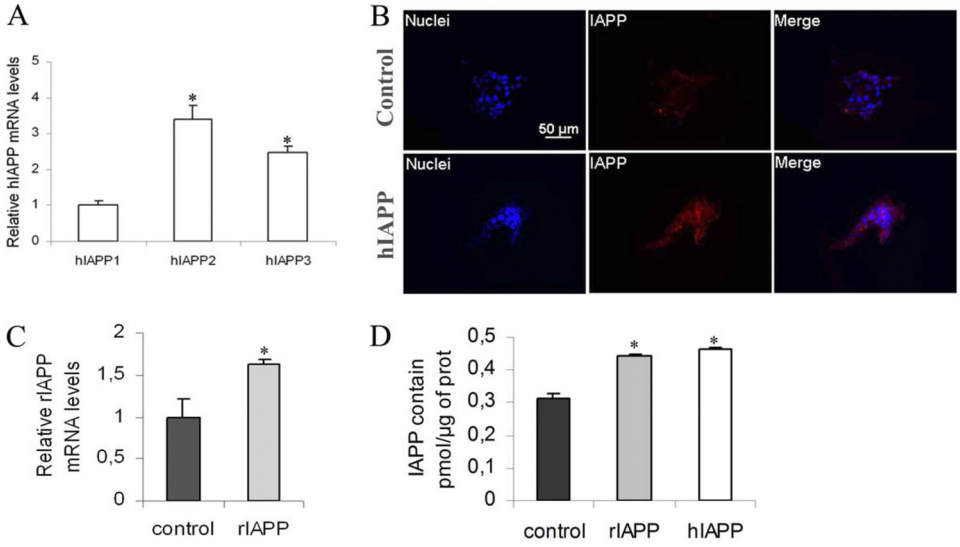

FIGURE 1. **Characterization of stable INS1E clones overexpressing hIAPP and rIAPP.** Cells were routinely cultured in RPMI medium at 11.1 mM glucose. *A*, hIAPP mRNA levels of stable INS1E clones were detected by real-time PCR. The data were normalized to GAPDH mRNA and presented as relative to the hIAPP1 cells *, $p < 0.05$ *versus* hIAPP1 cells ($n = 3$–5). *B*, specificity of hIAPP immunostaining. Immunodetection of hIAPP in control cells and hIAPP cells (×40); IAPP immunostaining is detected in the cytoplasm. *Bar* is 50 μm. *C*, rIAPP mRNA levels of stable INS1E clones were detected by real-time PCR. The data were normalized to GAPDH mRNA and presented as relative to control cells *, $p < 0.05$ *versus* control cells ($n = 3$–5). *D*, total IAPP content was measured by ELISA assay in cells cultured in routine culture medium (11.1 mM). *, $p < 0.05$ *versus* control cells ($n = 4$). Results are expressed as mean ± S.E.

Statistical Analysis

Data are expressed as mean ± S.E. for at least three independent experiments in duplicate. Variances in different groups were analyzed by Student's *t* test. *p* value <0.05 was accepted as significant.

RESULTS

Overexpression of hIAPP Alters Glucose-stimulated Insulin and IAPP Secretion—To investigate the effects of hIAPP overexpression on insulin secretion, a rat pancreatic beta-cell line, INS1E, was stably transfected with hIAPP cDNA (hIAPP cells) or the empty vector (control cells). Overexpression of hIAPP was confirmed by real-time PCR (Fig. 1*A*) and immunodetection (Fig. 1*B*). Three hIAPP-overexpressing clones were compared with the control clone. The hIAPP1 clone showed a lower hIAPP gene expression as compared with the other two clones (Fig. 1*A*). The overproduction of hIAPP protein was confirmed by immunostaining in the hIAPP3 clone. The hIAPP immunolabeling was observed in the cytoplasm, and the staining intensity was clearly stronger in hIAPP cells than in control cells (Fig. 1*B*).

To study the functionality of our cell clones, we have measured insulin and IAPP secretion in response to glucose. Insulin secretion from control cells at 16.7 mM glucose was increased 11-fold relative to secretion at 2.8 mM glucose, but in hIAPP cells, it was only stimulated 2-fold (Fig. 2*A*). Interestingly, hIAPP1 cells, which had the lowest hIAPP gene expression, showed a better capacity of insulin release in response to glucose than the two other clones. At 2.8 mM glucose, hIAPP cells showed a greater IAPP secretion relative to control cells (Fig. 2*B*). Nevertheless, in response to glucose, IAPP secretion was affected in the same way as insulin secretion in hIAPP cells as compared with control cells (Fig. 2*B*).

For the continuation of the study, we no longer used the hIAPP1, which had low hIAPP gene expression. As the other two hIAPP clones responded in a similar way to glucose, the following experiments were exclusively carried out in hIAPP3 cells. The defect in insulin secretion observed in hIAPP cells does not appear to be associated with a defect in the VCC activation because exposure of hIAPP cells to KCl induced a strong insulin secretion about 17-fold as in control cells (Fig. 2*C*). By electronic microscopy, at 2.8 mM glucose, we observed the presence of secretory vesicles associated to the plasmatic membrane in both clones (Fig. 2*D*, *panels a* and *c*). At 16.7 mM glucose, we observed few vesicles in control cells because insulin and IAPP had been already secreted in response to glucose (Fig. 2*D*, *panel b*), whereas hIAPP cells showed an accumulation of secretory vesicles at the plasma membrane (Fig. 2*D*, *panel d*). This result supports the existence of the defect of insulin secretion in hIAPP cells in response to glucose.

To confirm that defect of capacity of insulin release in hIAPP cells was specific for hIAPP overexpression, we have created another INS1E cell line that stably overexpressed rIAPP. Overexpression of rIAPP was confirmed by real-time PCR, and we observed an increase of rIAPP gene expression of about 1.6 times in rIAPP cells as compared with control cells (Fig. 1*C*). In rIAPP cells, IAPP protein levels were higher than control and similar to hIAPP cells (Fig. 1*D*). Insulin secretion from rIAPP cells at 16.7 mM glucose was increased 20-fold relative to secretion at 2.8 mM glucose and was similar to secretion from control cells in the same conditions (Fig. 2*A*). To confirm our results, we have overexpressed hIAPP gene in rat pancreatic islets by lentiviral transduction. The infection was effective, and hIAPP islets showed a strong hIAPP gene expression (Fig. 3*A*). We observed that insulin secretion in response to 16.7 mM glucose was decreased in hIAPP-overexpressed islets as compared with control islets (1.57 ± 0.09 *versus* 2.60 ± 0.26% insulin release expressed as a percentage of insulin content) (Fig. 3*B*). These data strongly support our results obtained in INS1E cells.

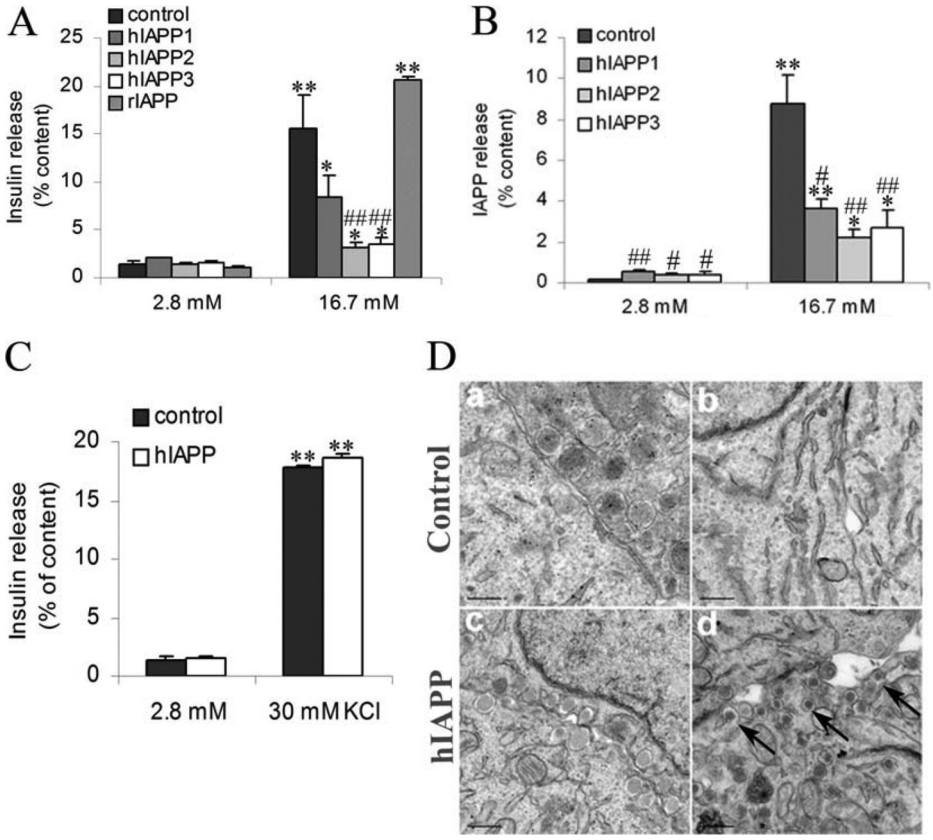

FIGURE 2. **Secretory capacity in response to glucose in stable INS1E clones.** *A* and *B*, 2 h before analyses, cells were depleted without glucose, after which insulin and IAPP release was measured following 1.5 h of incubation at basal 2.8 mM glucose and stimulatory 16.7 mM glucose. *C*, insulin secretion was also measured in the presence of 30 mM KCl. Insulin (*A* and *C*) and IAPP (*B*) secretion was tested in stable INS1E clones. Values were normalized to total cellular content of insulin and IAPP, respectively.*, $p < 0.05$; **, $p < 0.01$ *versus* secretion at 2.8 mM glucose; #, $p < 0.05$; ##, $p < 0.01$ *versus* corresponding control ($n = 5$). Results are expressed as mean ± S.E. *D*, electronic microscopy images from control and hIAPP cells. After 2 h of 2.8 mM glucose stimulation, secretory vesicles are detected in both clones (*panels a* and *c*). After 2 h of 16.7 mM glucose stimulation, secretory vesicles are not detected in control cells (*panel b*) but seem to be accumulated at the plasma membrane in hIAPP cells (arrows in *panel d*). *Bars* are 0.2 μm.

hIAPP-expressing Cells Present Immunoreactivity for Intracellular Oligomers—The immunogold labeling for oligomers was mostly detected in hIAPP cells as compared with control cells (1.78 ± 0.32 *versus* 0.53 ± 0.10 gold particle number/μm^2) and was reinforced in the cytoplasm in association with the endoplasmic reticulum (ER). Moreover, a few oligomer immunogold particles were also observed in insulin granules and close to the plasma membrane in hIAPP cells (Fig. 4). It has been previously suggested that oligomers were the toxic form of IAPP causing the apoptosis of beta-cells (27, 36). In our culture conditions, there was no change in cell death (supplemental Fig. S1) and in the expression of genes involved in ER stress (supplemental Fig. S2) in hIAPP cells as compared with control cells.

hIAPP Cells Fail to Mobilize Intracellular Ca^{2+} in Response to Glucose—It is well known that calcium is an essential trigger for the exocytosis of insulin granules. At 2.8 mM glucose, hIAPP cells showed a greater $[Ca^{2+}]_i$ than control cells (Fig. 5*A*). Consistent with a defective insulin secretion, the study of calcium signals demonstrated an absence of response to glucose in hIAPP cells. Although 76.61% of control cells tested (194/201) exhibited a normal Ca^{2+} mobilization in response to 16.7 mM glucose, none of the hIAPP cells tested were able to respond to glucose (0/192) (Fig. 5*B*). As we have shown for insulin secretion response, the exposure of hIAPP cells to KCl induced a strong increase of intracellular Ca^{2+} concentration (Fig. 5*B*). Therefore, the defect that inhibits GSIS must be upstream of VCC activation.

Coupling Efficiency of Oxidative Phosphorylation Is Unaltered in hIAPP Cells—Because mitochondria are key determinants in GSIS, we investigated the respiratory capacity of our stable INS1E cell lines. hIAPP cells had the same respiratory rate relative to controls at 2.8 mM, and in response to 16.7 mM glucose stimulation, O_2 consumption increased to the same extent in both clones (Fig. 6). After the addition of oligomycin, an inhibitor of ATP synthase, the remaining consumption of oxygen, which represents the endogenous proton leak activity, was identical in both cell lines (Fig. 6). We have also calculated the coupling efficiency (percentage of respiratory activity used to synthesize ATP), which corresponds to the difference between oxygen consumption in basal and oligomycin-treated conditions, and it was similar (about 40%) in hIAPP and control cells. In accordance with these data, we did not observe a difference in ATP levels between hIAPP and control cells (Fig. 7*C*). Moreover, the ratio of mitochondrial to cytoplasmic DNA, which reflects the mitochondria content (supplemental Fig. S3), and the expression of genes involved in mitochondrial biogenesis (mitochondrial transcription factor A (TFAM) and nuclear respiratory factor 1 (NRF1)) were similar between both cell clones (supplemental Fig. S2). Moreover, we did not

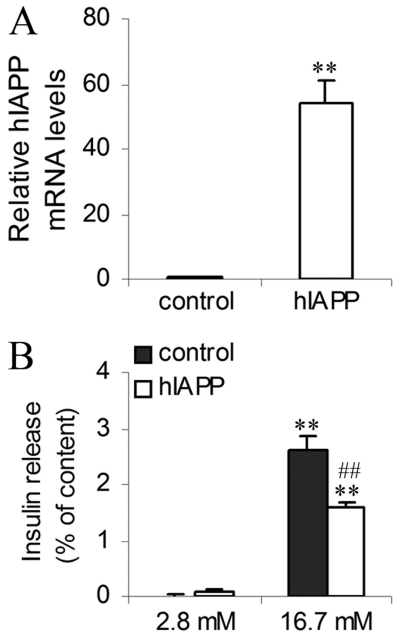

FIGURE 3. **Characterization and secretory capacity of islets overexpressing hIAPP.** Islets were cultured in RPMI medium at 5.5 mM glucose. *A*, hIAPP mRNA levels of islets overexpressing hIAPP (hIAPP islets) were detected by real-time PCR. The data were normalized to GAPDH mRNA and presented as relative to control islets infected by pLenti-LacZ (control islets). **, $p < 0.01$ *versus* control islets ($n = 3$). *B*, 2 h before analyses, islets were depleted without glucose, after which insulin release was measured following 1.5 h of incubation at basal 2.8 mM glucose and stimulatory 16.7 mM glucose. Insulin secretion was tested in islets infected by pLenti-LacZ or pLenti-hIAPP. Values were normalized to total cellular content of insulin. **, $p < 0.01$ *versus* secretion at 2.8 mM glucose; ##, $p < 0.01$ *versus* corresponding control ($n = 3$). Results are expressed as mean ± S.E.

observe any changes in the protein expression of mitochondrial respiratory chain subunits (supplemental Fig. S4).

Maximal Respiratory Capacity and Mitochondrial Membrane Potential Are Increased in hIAPP Cells—FCCP is a chemical uncoupler that can completely uncouple mitochondria and maximize their respiratory capacity. Thus, the FCCP-stimulated O_2 consumption reflects the maximal capacity of the electron transport system. FCCP-stimulated O_2 consumption is increased in the hIAPP cells as compared with controls (79.62 ± 8.84 *versus* 46.56 ± 6.25 pmol/s/million of cells) (Fig. 6). Mitochondrial membrane potential ($\Delta\psi_m$) reflects the activity of the electron transport system. In agreement with the previous result, hIAPP cells exhibited a significantly increased mitochondrial membrane potential relative to control cells, which is represented by a greater decrease of probe fluorescence (ΔF) in response to glucose stimulation (35.97 ± 1.45 *versus* 20.43 ± 1.73% of decrease relative to 2.8 mM glucose, $p < 0.05$) (Fig. 7*A*). $\Delta\psi_m$ is an important regulator of mitochondrial ROS, and the generation of ROS is exponentially dependent on $\Delta\psi_m$ (37). In agreement with these data, ROS levels were greater in hIAPP than control cells (Fig. 7*B*) under glucose stimulation. We then investigated the key step between the ATP production and the opening of VCC: the closure of K_{ATP} channels.

hIAPP Cells Fail to Mobilize Intracellular Ca^{2+} in Response to Sulfonylurea—We explored the activity of the K_{ATP} channel in a glucose-independent manner, using a sulfonylurea drug, tolbutamide. This compound stimulates insulin secretion by binding to K_{ATP} channels and inducing their closure. Consistent with a defect in K_{ATP} channel function, hIAPP cells responded poorly to tolbutamide (Fig. 8*A*). Indeed, whereas 97.05% of control cells (132/136) showed a normal response to tolbutamide, only 9.6% of hIAPP cells (9/93) were able to respond (Fig. 8*B*). Because K_{ATP} channel activity is mostly regulated at the transcriptional level, we measured the gene expression of the channel subunits. There was no difference in the expression of Kir6.2 or SUR1 genes between control and hIAPP cells (supplemental Fig. S2).

DISCUSSION

Amyloid deposition is a recognized hallmark of the islets of type 2 diabetic patients, with the main component of amyloid deposits being the islet amyloid polypeptide. There is strong evidence supporting the key role of amyloidogenesis in the progressive loss of pancreatic beta-cell function and mass. In this study, we generated rat pancreatic INS1E beta-cell lines that stably overexpressed the human *IAPP* gene. In addition to human *IAPP* gene expression, these cells also showed an increase presence of IAPP protein, but they failed to show apoptosis under the conditions present in our study. This result is not in accordance with a recent study involving COS-1 cells, which showed that transient hIAPP overexpression induced apoptosis (38). The difference in results could be due to the different cellular models used; COS-1 cells are derived from kidney cells, whereas INS1E cells are derived from pancreatic beta-cells. In accordance with previous works reviewed (39), the overexpression of hIAPP in our study induced the formation of intracellular amyloid oligomers, detected by the A11 antibody. This antibody has been well described and characterized (27) and has been used in various recent studies (28, 40). Nevertheless, the specificity of the antibody was questioned. Indeed, Yoshiike *et al.* (41) have demonstrated that A11 antibody also bound natively folded proteins such as heat shock proteins, and on the contrary, Lin *et al.* (42) proved the specificity of this antibody in detecting toxic oligomers in islets of hIAPP, but not in rIAPP transgenic mice. In agreement with these last data, in our model, the difference between control cells, which only express rIAPP, and hIAPP-expressing cells is strongly significant. In addition, our results are also in agreement with the data published by Gurlo *et al.* (28) that showed the presence of oligomer labeling in the cytoplasm in association with the ER. Nevertheless, despite the presence of these deposits, we did not detect ER stress in the hIAPP cells, which supports the findings of a study on hIAPP transgenic mice in which the authors demonstrated that amyloid formation was not associated with significant increases in the expression of ER stress markers (43).

We reported here that hIAPP cells showed a failure in insulin and IAPP secretion in response to glucose stimulation, whereas rIAPP cells did not present these defects. Unlike hIAPP, rIAPP is a non-amyloidogenic form that does not accumulate and does not induce oligomer and/or fibril deposition in beta-cells (5). Our results prove that hIAPP overexpression specifically induces the defect in insulin secretion, possibly due to its capacity to aggregate and form intracellular oligomers. In addition, to confirm our results, we have overexpressed hIAPP in rat pancreatic islets using lentiviral infection, which allowed us to

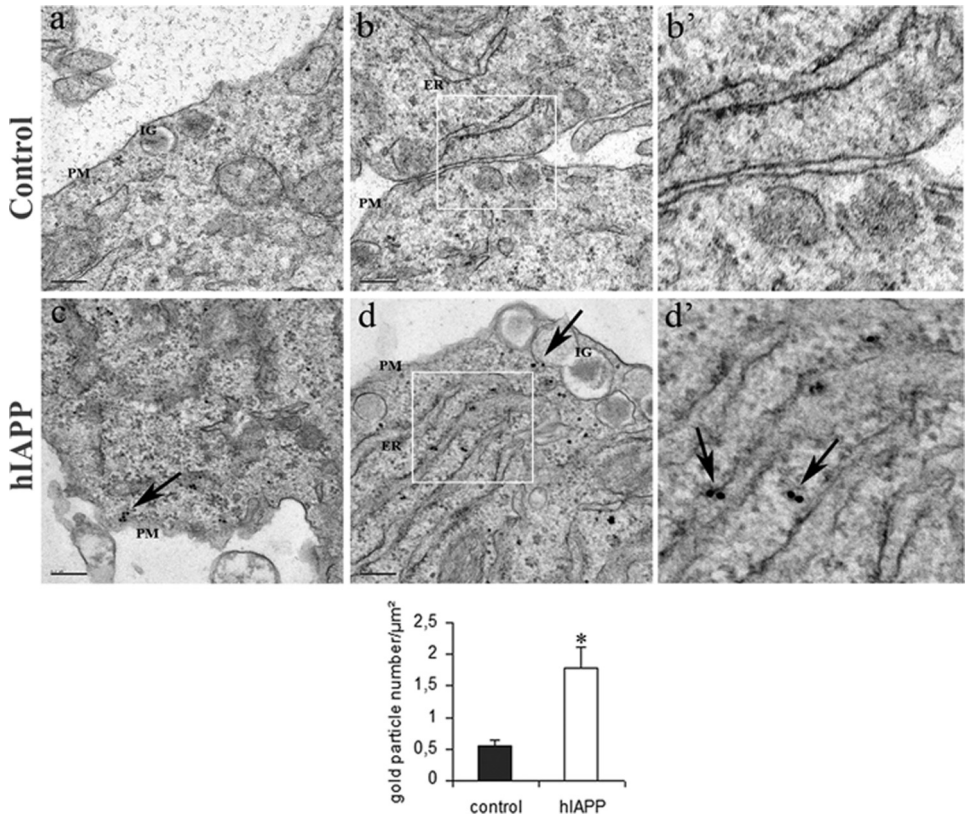

FIGURE 4. **Cellular localization of intracellular oligomers in hIAPP cells.** Immunogold labeling for oligomers in hIAPP-non-expressing cells (control) (*panels a*, *b*, and *b'*) and hIAPP-expressing cells (hIAPP cells) (*panels c*, *d*, and *d'*) is shown; *panels b'* and *d'* were enlargements of *panels b* and *d*, respectively. Oligomers were only detected in hIAPP cells in the ER (*arrows* in *panel d'*), in insulin granules (*IG*) (*arrow* in *panel d*), and associated to the plasma membrane (*PM*) (*arrow* in *panel c*). *Bars* are 0.2 μm. *, $p < 0.05$ *versus* control cells.

obtain a long term hIAPP overexpression. The results obtained in primary cells strongly reinforced our data in INS1E cells, demonstrating that hIAPP overexpression altered insulin secretion in response to glucose.

Different studies have demonstrated that IAPP can inhibit GSIS (13–15); however, the mechanism has not been established. To gain insight into the mechanisms underlying this defective secretory response, we explored intracellular calcium levels and their mobilization in response to glucose. In agreement with many previous studies, we reported an increase in intracellular Ca^{2+} in hIAPP cells as compared with controls. The mechanisms described previously include the direct formation of Ca^{2+}-permeable pores by the amyloid oligomers themselves and the activation of VCC (11, 44) in the plasma membrane and/or in the ER. Indeed, it has been shown that hIAPP overexpression provokes the formation of intracellular oligomers (28, 38) and that amyloid oligomers increase intracellular Ca^{2+} in neurons and astrocytes (45–48). Zhu *et al*. (29) have demonstrated that high concentrations of hIAPP inhibited the activity of VCC, leading to a defect in the intracellular Ca^{2+} mobilization in pancreatic islets, and they suggested that this could explain the failure in GSIS. In accordance with these data, our hIAPP cells, which showed high hIAPP protein levels, failed to increase intracellular Ca^{2+} in response to glucose. Nevertheless, in our model, this defect did not appear to be associated with a failure of Ca^{2+} channel activity as exposure of hIAPP cells to KCl induced robust intracellular Ca^{2+} mobilization and also insulin secretion. Indeed, KCl induced a depolarization of the plasma membrane and consequently induced Ca^{2+} mobilization, independently of the closure of K_{ATP} channels.

Because mitochondrial defects in beta-cells perturb GSIS and might be associated with diabetes (49, 50), we investigated the mitochondrial metabolism in our clones. The coupling efficiency of oxidative phosphorylation can be defined as the part of the mitochondrial respiratory rate that is used for ATP production. In agreement with a previous study (51), we showed that INS1E cells exhibited a high proton leak activity, which was observed following the addition of an ATP synthase inhibitor, oligomycin. Thus, the coupling efficiency (about 40%) was low as compared with values reported for other mammalian (and non-mammalian) cells. Moreover, the coupling efficiency was similar in our hIAPP and control cells, as with the ATP levels. It is known that the concentration of ATP remains nearly constant in beta-cells, with small changes in ATP concentrations as a characteristic feature of the response of beta-cells to glucose stimulation (52). Thus, it is very difficult to detect any differences in ATP concentrations, taking into consideration the data of ATP concentrations in beta-cell models.

The maximal respiratory capacity measured in the presence of excess chemical uncoupler FCCP was higher in hIAPP cells than in control cells. This result was in accordance with the high $\Delta\psi_m$ reflecting electron transport system capacity. Our results are not in accordance with recent studies showing that

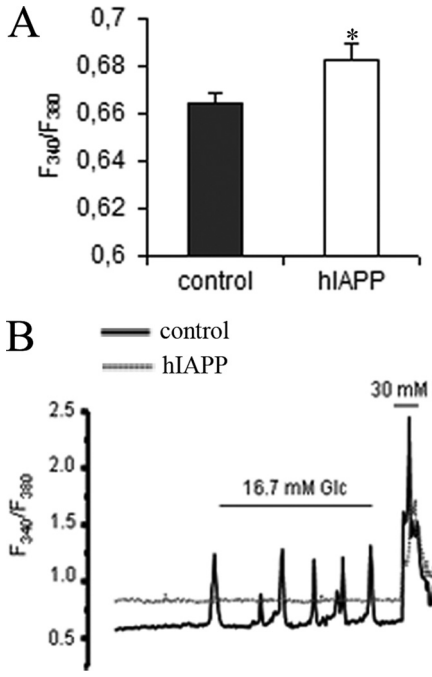

FIGURE 5. **Intracellular Ca^{2+} signals clones in response to glucose in stable INS1E.** Cells were cultured overnight at 2.8 mM glucose before analyses. Intracellular Ca^{2+} levels were detected with fura 2-AM fluorescent probe. *A*, basal intracellular Ca^{2+} concentrations were measured at basal 2.8 mM glucose. *, $p < 0.05$ *versus* control cells ($n = 192–201$). Results are expressed as mean ± S.E. *B*, representative diagram of measurement of intracellular calcium in response to the addition of 16.7 mM glucose and 30 mM KCl. Fluorescence changes are expressed as the ratio of fluorescence at 340 and 380 nm (F_{340}/F_{380}).

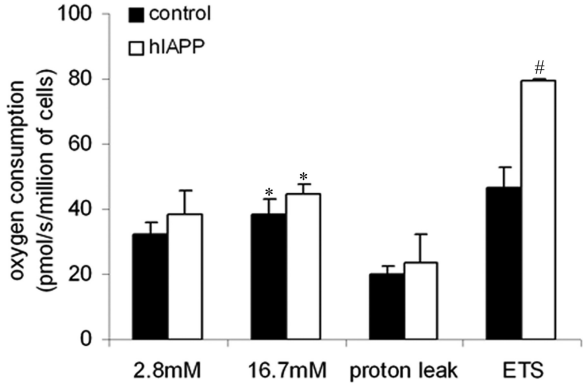

FIGURE 6. **Mitochondrial respiratory capacity and coupling efficiency in stable INS1E clones.** Cells were cultured overnight at 2.8 mM glucose before analyses. Cells were placed into an oxymeter chamber and stabilized for at least 10 min. O_2 consumption was measured at 2.8 and 16.7 mM glucose by raising the glucose concentration directly in the oxymeter chamber without any drugs. Then, the uncoupled respiration was tested by the addition of oligomycin, and the maximal respiratory capacity was measured in the presence of FCCP. *, $p < 0.05$ *versus* O_2 consumption at 2.8 mM glucose. #, $p < 0.05$ *versus* control cells ($n = 8$). Results are expressed as mean ± S.E.

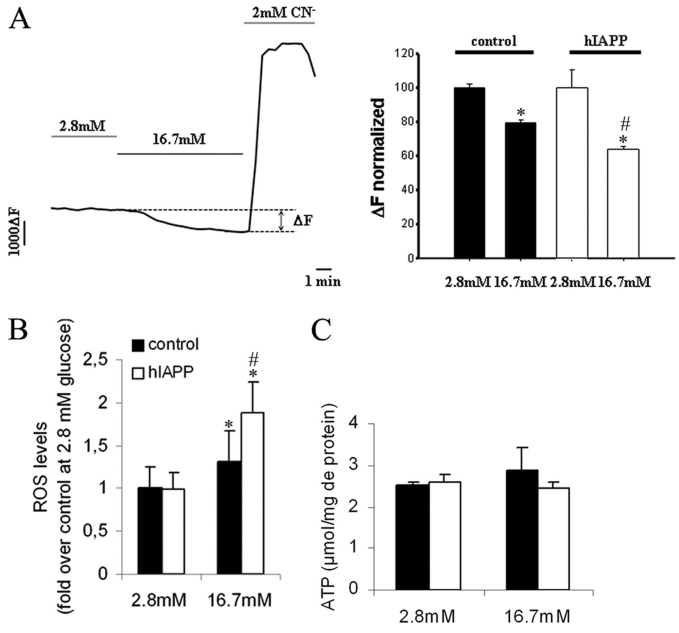

FIGURE 7. **$\Delta\psi_m$, ROS, and ATP levels in stable INS1E clones.** Cells were cultured overnight at 2.8 mM glucose before analyses. *A*, $\Delta\psi_m$ was monitored as rhodamine-123 fluorescence, and hyperpolarization was induced by raising glucose from basal 2.8 mM to stimulatory 16.7 mM. Complete depolarization of the mitochondrial membrane was induced by the addition of 2 mM of the mitochondrial toxicant cyanide (CN^-). *, $p < 0.05$ *versus* $\Delta\psi_m$ at 2.8 mM glucose; #, $p < 0.05$ *versus* corresponding control cells ($n = 139–150$). *B*, ROS levels were measured following a 2-h incubation at 16.7 mM glucose using CM-H_2DCFDA fluorescent probe. *, $p < 0.05$ *versus* ROS level at 2.8 mM glucose; #, $p < 0.05$ *versus* corresponding control cells ($n = 6$). *C*, ATP levels were measured following a 30-min incubation at 16.7 mM glucose using a luciferin-luciferase bioluminescent assay ($n = 3–5$). Results are expressed as mean ± S.E.

extracellular treatment with hIAPP induced mitochondrial dysfunction. Indeed, Li *et al.* (53) showed that extracellular treatment with hIAPP reduced intracellular ATP content and $\Delta\psi_m$ in INS1E cells. Furthermore, Lim *et al.* (54) showed that amyloid β, which is involved in the neuronal loss that takes place in Alzheimer disease, and hIAPP share a common pathway by inhibiting the activity of the mitochondrial complex IV. This disagreement could be explained by different cellular responses to the presence of extracellular fibrils or intracellular oligomers, especially because it has already been described that the two forms of amyloid deposits do not have the same cellular actions (36). A change in $\Delta\psi_m$ could be explained by a modulation of "$\Delta\psi_m$ producer" (*i.e.* the mitochondrial respiratory chain) and/or "$\Delta\psi_m$ consumer" (*i.e.* either phosphorylation or endogenous proton leak activity) (51). We have observed that there was no increase in $\Delta\psi_m$ consumers because the coupling efficiency and the endogenous proton leak activity were similar in both clones. Although we did not show changes in the expression of OXPHOS proteins, there could be an increase in the activity of these components in hIAPP cells, in particular complex I, which is the major site of ROS production. Indeed, hIAPP cells showed higher ROS levels than control cells. These results are in accordance with a study by Zraika *et al.* (55), who demonstrated that hIAPP transgenic islets cultured in 16.7 mM glucose showed elevated ROS levels in relation to control islets cultured under the same conditions. An explanation consistent with our results could involve the elevated $\Delta\psi_m$ in hIAPP cells. It has been shown that the generation of ROS is exponentially dependent on $\Delta\psi_m$ (37). ROS generation correlates well with metabolic rates, suggesting that a faster metabolism simply results in more respiratory chain leakage (56, 57). Indeed, several recent studies showed that mitochondrial ROS could be a good candidate for rapidly regulating pathways that depend directly on metabolic fluxes. Among others, Leloup *et al.* (58) demonstrated that glucose-induced mitochondrial ROS production is an obligatory stimulus for insulin secretion, although

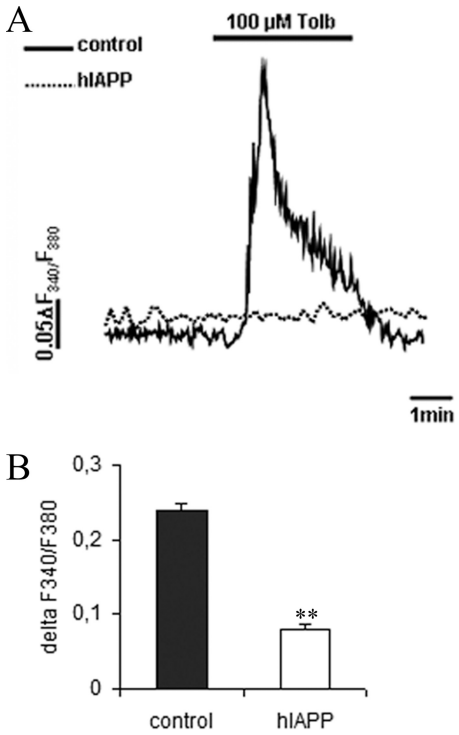

FIGURE 8. **Intracellular Ca^{2+} signals in response to sulfonylurea drug in stable INS1E clones.** Cells were cultured overnight at 2.8 mM glucose before analysis. Intracellular Ca^{2+} levels were detected with fura 2-AM fluorescent probe. *A*, representative diagram of a measurement of intracellular calcium in response to 100 μM tolbutamide (*Tolb*). *B*, intracellular Ca^{2+} mobilization in response to 100 μM tolbutamide. Values represent the difference of the ratio F_{340}/F_{380} between the minimum and the maximum tolbutamide stimulation (n = 192–201). **, $p < 0.01$ *versus* control cells. Results are expressed as mean ± S.E.

the mechanism leading to insulin secretion has not been identified. Therefore, it is possible that activation of mitochondrial metabolism linked to the increase in ROS production can be used by hIAPP cells as a defense mechanism to counteract the defect in insulin secretion.

Elevated ROS levels can lead to the progressive loss of beta-cell function and contribute to the development of type 2 diabetes by impairing GSIS (59, 60). Keeping these data in mind, high ROS levels in hIAPP could provide an explanation for the defect in insulin secretion in response to glucose that we have observed in this present study. Nevertheless, at 2.8 mM glucose, a condition under which we did not observe elevated ROS levels, we observed a defect in Ca^{2+} mobilization in response to tolbutamide in hIAPP cells, as compared with controls. The elevated ROS production could not justify the defect of Ca^{2+} mobilization in response to tolbutamide. This molecule is a sulfonylurea drug that binds directly to K_{ATP} channels and induces insulin secretion, independently of any changes in cellular metabolic status. Our results strongly suggest that the functionality of the K_{ATP} channel was impaired in hIAPP cells, in agreement with the study led by Salas *et al.* (13) that showed that IAPP inhibits insulin secretion in response to sulfonylurea in a perfused rat pancreas. Although further investigation is needed to demonstrate the precise mechanism by which hIAPP affects K_{ATP} channel activity, we propose that hIAPP oligomers could be involved in altering the binding of tolbutamide or ATP within the channel. This hypothesis is supported by recent data published by Zhu *et al.* (29), which demonstrate that hIAPP inhibits the activity of ions channels probably by a direct effect.

Our study sheds new light on the mechanisms by which hIAPP inhibits insulin secretion. We conclude that hIAPP alters K_{ATP} channel activity, leading to a defect in insulin and IAPP secretion in response to glucose. The increase in mitochondrial activity may be a compensatory mechanism for counteracting these defects.

Acknowledgments—We thank Donald McDonagh (from CIBERDEM Secretariat) for language consultancy. We are grateful to Pablo M. Garcia-Roves and Nathalie Nicod for valuable help in the preparation of the manuscript. We also thank Dr. Antonio Zorzano for scientific council.

REFERENCES

1. Kasuga, M. (2006) *J. Clin. Invest.* **116,** 1756–1760
2. Prentki, M., and Nolan, C. J. (2006) *J. Clin. Invest.* **116,** 1802–1812
3. Clark, A., Cooper, G. J., Lewis, C. E., Morris, J. F., Willis, A. C., Reid, K. B., and Turner, R. C. (1987) *Lancet* **2,** 231–234
4. Westermark, P., Wernstedt, C., Wilander, E., Hayden, D. W., O'Brien, T. D., and Johnson, K. H. (1987) *Proc. Natl. Acad. Sci. U.S.A.* **84,** 3881–3885
5. Betsholtz, C., Christmanson, L., Engström, U., Rorsman, F., Jordan, K., O'Brien, T. D., Murtaugh, M., Johnson, K. H., and Westermark, P. (1990) *Diabetes* **39,** 118–122
6. Gasa, R., Gomis, R., Casamitjana, R., and Novials, A. (1997) *Regul. Pept.* **68,** 99–104
7. Kahn, S. E., D'Alessio, D. A., Schwartz, M. W., Fujimoto, W. Y., Ensinck, J. W., Taborsky, G. J., Jr., and Porte, D., Jr. (1990) *Diabetes* **39,** 634–638
8. Novials, A., Sarri, Y., Casamitjana, R., Rivera, F., and Gomis, R. (1993) *Diabetes* **42,** 1514–1519
9. Janson, J., Ashley, R. H., Harrison, D., McIntyre, S., and Butler, P. C. (1999) *Diabetes* **48,** 491–498
10. Lorenzo, A., Razzaboni, B., Weir, G. C., and Yankner, B. A. (1994) *Nature* **368,** 756–760
11. Mirzabekov, T. A., Lin, M. C., and Kagan, B. L. (1996) *J. Biol. Chem.* **271,** 1988–1992
12. Casas, S., Gomis, R., Gribble, F. M., Altirriba, J., Knuutila, S., and Novials, A. (2007) *Diabetes* **56,** 2284–2294
13. Salas, M., Silvestre, R. A., Garcia-Hermida, O., Fontela, T., Rodriguez-Gallardo, J., and Marco, J. (1995) *Diabete Metab.* **21,** 269–273
14. Ohsawa, H., Kanatsuka, A., Yamaguchi, T., Makino, H., and Yoshida, S. (1989) *Biochem. Biophys. Res. Commun.* **160,** 961–967
15. Ahrén, B., Oosterwijk, C., Lips, C. J., and Höppener, J. W. (1998) *Diabetologia* **41,** 1374–1380
16. Aguilar-Bryan, L., and Bryan, J. (1999) *Endocr. Rev.* **20,** 101–135
17. Ashcroft, F. M., and Gribble, F. M. (1999) *Diabetologia* **42,** 903–919
18. Seino, S. (1999) *Annu. Rev. Physiol.* **61,** 337–362
19. Flanagan, S. E., Patch, A. M., Mackay, D. J., Edghill, E. L., Gloyn, A. L., Robinson, D., Shield, J. P., Temple, K., Ellard, S., and Hattersley, A. T. (2007) *Diabetes* **56,** 1930–1937
20. Gloyn, A. L., Reimann, F., Girard, C., Edghill, E. L., Proks, P., Pearson, E. R., Temple, I. K., Mackay, D. J., Shield, J. P., Freedenberg, D., Noyes, K., Ellard, S., Ashcroft, F. M., Gribble, F. M., and Hattersley, A. T. (2005) *Hum. Mol. Genet* **14,** 925–934
21. Flanagan, S. E., Clauin, S., Bellanné-Chantelot, C., de Lonlay, P., Harries, L. W., Gloyn, A. L., and Ellard, S. (2009) *Hum. Mutat.* **30,** 170–180
22. Thomas, P., Ye, Y., and Lightner, E. (1996) *Hum. Mol. Genet* **5,** 1809–1812
23. Thomas, P. M., Cote, G. J., Wohllk, N., Haddad, B., Mathew, P. M., Rabl, W., Aguilar-Bryan, L., Gagel, R. F., and Bryan, J. (1995) *Science* **268,** 426–429
24. Craig, T. J., Ashcroft, F. M., and Proks, P. (2008) *J. Gen. Physiol.* **132,** 131–144
25. Zraika, S., Hull, R. L., Verchere, C. B., Clark, A., Potter, K. J., Fraser, P. E.,

Raleigh, D. P., and Kahn, S. E. (2010) *Diabetologia* **53,** 1046–1056
26. Glabe, C. G., and Kayed, R. (2006) *Neurology* **66,** S74–78
27. Kayed, R., Head, E., Thompson, J. L., McIntire, T. M., Milton, S. C., Cotman, C. W., and Glabe, C. G. (2003) *Science* **300,** 486–489
28. Gurlo, T., Ryazantsev, S., Huang, C. J., Yeh, M. W., Reber, H. A., Hines, O. J., O'Brien, T. D., Glabe, C. G., and Butler, P. C. (2010) *Am. J. Pathol.* **176,** 861–869
29. Zhu, T., Wang, Y., He, B., Zang, J., He, Q., and Zhang, W. (2011) *Diabetes Metab. Res. Rev.* **27**, 28–34
30. Gasa, R., Gomis, R., Casamitjana, R., Rivera, F., and Novials, A. (1997) *Am. J. Physiol.* **272,** E543–E549
31. Novials, A., Mato, E., Lucas, M., Franco, C., Rivas, M., Santisteban, P., and Gomis, R. (2004) *Diabetologia* **47,** 1167–1174
32. Becker, T. C., Noel, R. J., Coats, W. S., Gómez-Foix, A. M., Alam, T., Gerard, R. D., and Newgard, C. B. (1994) *Methods Cell Biol.* **43,** 161–189
33. Soriano, S., Gonzalez, A., Marroquí, L., Tudurí, E., Vieira, E., Amaral, A. G., Batista, T. M., Rafacho, A., Boschero, A. C., Nadal, A., Carneiro, E. M., and Quesada, I. (2010) *Endocrinology* **151,** 3543–3554
34. Pertusa, J. A., Nesher, R., Kaiser, N., Cerasi, E., Henquin, J. C., and Jonas, J. C. (2002) *Diabetes* **51,** 2552–2560
35. Ravnskjaer, K., Boergesen, M., Rubi, B., Larsen, J. K., Nielsen, T., Fridriksson, J., Maechler, P., and Mandrup, S. (2005) *Endocrinology* **146,** 3266–3276
36. Meier, J. J., Kayed, R., Lin, C. Y., Gurlo, T., Haataja, L., Jayasinghe, S., Langen, R., Glabe, C. G., and Butler, P. C. (2006) *Am. J. Physiol. Endocrinol. Metab.* **291,** E1317–E1324
37. Starkov, A. A., and Fiskum, G. (2003) *J. Neurochem.* **86,** 1101–1107
38. Hiddinga, H. J., and Eberhardt, N. L. (1999) *Am. J. Pathol.* **154,** 1077–1088
39. Haataja, L., Gurlo, T., Huang, C. J., and Butler, P. C. (2008) *Endocr. Rev.* **29,** 303–316
40. Zhao, H. L., Sui, Y., Guan, J., He, L., Gu, X. M., Wong, H. K., Baum, L., Lai, F. M., Tong, P. C., and Chan, J. C. (2009) *Transl. Res.* **153,** 24–32
41. Yoshiike, Y., Minai, R., Matsuo, Y., Chen, Y. R., Kimura, T., and Takashima, A. (2008) *PLoS One* **3,** e3235
42. Lin, C. Y., Gurlo, T., Kayed, R., Butler, A. E., Haataja, L., Glabe, C. G., and Butler, P. C. (2007) *Diabetes* **56,** 1324–1332
43. Hull, R. L., Zraika, S., Udayasankar, J., Aston-Mourney, K., Subramanian, S. L., and Kahn, S. E. (2009) *Diabetologia* **52,** 1102–1111
44. Blanchard, B. J., Chen, A., Rozeboom, L. M., Stafford, K. A., Weigele, P., and Ingram, V. M. (2004) *Proc. Natl. Acad. Sci. U.S.A.* **101,** 14326–14332
45. Demuro, A., Mina, E., Kayed, R., Milton, S. C., Parker, I., and Glabe, C. G. (2005) *J. Biol. Chem.* **280,** 17294–17300
46. Kawahara, M., Kuroda, Y., Arispe, N., and Rojas, E. (2000) *J. Biol. Chem.* **275,** 14077–14083
47. Mattson, M. P., Cheng, B., Davis, D., Bryant, K., Lieberburg, I., and Rydel, R. E. (1992) *J. Neurosci.* **12,** 376–389
48. Mattson, M. P., and Goodman, Y. (1995) *Brain Res.* **676,** 219–224
49. Lowell, B. B., and Shulman, G. I. (2005) *Science* **307,** 384–387
50. Maechler, P., and Wollheim, C. B. (2001) *Nature* **414,** 807–812
51. Affourtit, C., and Brand, M. D. (2009) *Methods Enzymol.* **457,** 405–424
52. Ronner, P., Naumann, C. M., and Friel, E. (2001) *Diabetes* **50,** 291–300
53. Li, X. L., Chen, T., Wong, Y. S., Xu, G., Fan, R. R., Zhao, H. L., and Chan, J. C. (2011) *Int. J. Biochem. Cell Biol.* **43,** 525–534
54. Lim, Y. A., Rhein, V., Baysang, G., Meier, F., Poljak, A., Raftery, M. J., Guilhaus, M., Ittner, L. M., Eckert, A., and Götz, J. (2010) *Proteomics* **10,** 1621–1633
55. Zraika, S., Hull, R. L., Udayasankar, J., Aston-Mourney, K., Subramanian, S. L., Kisilevsky, R., Szarek, W. A., and Kahn, S. E. (2009) *Diabetologia* **52,** 626–635
56. Perez-Campo, R., López-Torres, M., Cadenas, S., Rojas, C., and Barja, G. (1998) *J. Comp. Physiol. B* **168,** 149–158
57. Sohal, R. S., and Allen, R. G. (1985) *Basic Life Sci.* **35,** 75–104
58. Leloup, C., Tourrel-Cuzin, C., Magnan, C., Karaca, M., Castel, J., Carneiro, L., Colombani, A. L., Ktorza, A., Casteilla, L., and Pénicaud, L. (2009) *Diabetes* **58,** 673–681
59. Coordt, M. C., Ruhe, R. C., and McDonald, R. B. (1995) *Proc. Soc. Exp. Biol. Med.* **209,** 213–222
60. Simmons, R. A., Suponitsky-Kroyter, I., and Selak, M. A. (2005) *J. Biol. Chem.* **280,** 28785–28791